Journal of Materials Chemistry C

ROYAL SOCIETY OF CHEMISTRY

PAPER

View Article Online
View Journal | View Issue

Cite this: *J. Mater. Chem. C*, 2024, **12**, 9784

Modulation of phosphor luminescence performance by high concentration self-sensitization of Er and Ho–Yb ion co-doping under 1550 nm excitation

Bohan Lei, Liping Lu * and Haiying Sun

In this paper, upconversion fluoride phosphors $NaY_{1-x-y-z}F_4:Er_x^{3+}$, Ho_y^{3+}, Yb_z^{3+} were synthesized by the low-temperature combustion method. And the optimal ratio of lanthanide ion doping in the matrix lattice was determined by the control variable method. First of all, the experimental results show that some Er^{3+}-2 ions may be present in the samples doped with a high concentration of Er^{3+} ions, and the energy carried by the 1550 nm photons is absorbed by them and transferred to the remaining Er^{3+}-1 ions in the form of sensitizers, which leads to saturation excitation of these Er^{3+}-1 ions. Thus, the upconversion luminescence intensity of the Er^{3+} ion-doped samples was dramatically increased. Secondly, it was found that the singly doped Ho^{3+} ion samples also showed significant absorption of 1550 nm photons. In contrast, doping Yb^{3+} ions in samples singly doped with Ho^{3+} ions produces the opposite effect of Er^{3+} ions. The upconversion luminescence intensity of the Ho^{3+} ion-doped samples is significantly quenched. According to the above experimental phenomena, when a small amount of Ho^{3+} ions are doped into the matrix lattice of the sample doped with a high concentration of Er^{3+} ions, firstly, these Ho^{3+} ions can act as transient energy transition centers in the lattice. Secondly, they can also play the role of another self-absorption activation center in the matrix lattice. The upconversion luminescence performance of the Er^{3+}–Ho^{3+} ion co-doped samples is significantly enhanced, so the characteristic emissions of Er^{3+} and Ho^{3+} ions are highly overlapped in the visible region. A small amount of Yb^{3+} ions continue to be doped into the Er^{3+}–Ho^{3+} ion co-doped system, due to the significant quenching effect of the Yb^{3+} ions on the luminescence of the Ho^{3+} ions. The Yb^{3+} ions mainly play the role of reverse energy transfer centers between the Er^{3+}–Yb^{3+} ions in the crystal lattice. This results in the upconversion luminescence intensity of the triple-doped samples being enhanced significantly by increasing the utilization of the system for the 1550 nm photons. In this paper, the phase composition and morphology of the phosphors were studied by an X-ray diffractometer and scanning electron microscope. The upconversion luminescence mechanism of Er^{3+}–Ho^{3+}–Yb^{3+} ion triple-doped samples under 1550 nm excitation and the sensitization interactions between the ions were systematically investigated by upconversion emission spectra and fluorescence lifetime. This work provides a new idea for the design of high-color purity upconversion luminescent phosphors under 1550 nm excitation, and the prepared phosphors can be applied in the field of display lighting.

Received 4th March 2024,
Accepted 27th May 2024

DOI: 10.1039/d4tc00859f

rsc.li/materials-c

1. Introduction

Upconversion luminescence is an anti-Stokes process by which low-energy infrared light can be converted into high-energy visible light.[1] Therefore, it has been widely studied in infrared detection, optical anti-counterfeiting, and bio-detection.[2–4] Currently, the research on upconversion luminescence is mainly concentrated in the 980 nm band,[5] but the research on the 1550 nm band is relatively rare. This is mainly due to the lack of effective sensitizer ions in the 1550 nm band.[6] However, compared with the 980 nm band, the 1550 nm band has strong anti-interference ability, strong anti-light scattering ability, and safety for living organisms.[7] Hence, the 1550 nm band has better application prospects. Among lanthanide ions, Er^{3+} ions have the largest absorption cross-section for 1550 nm photons, so Er^{3+} ions have potential as sensitizer ions in this band.[6] However, if only relying on the doping of Er^{3+} ions to achieve a good response of the matrix lattice to 1550 nm photons, it will inevitably lead to an increase in the doping concentration of

School of Materials Science and Engineering, Changchun University of Science and Technology, Changchun 130022, China. E-mail: luliping771219@126.com

Er^{3+} ions.[8] In addition, the upconversion luminescence intensity of the samples under 1550 nm excitation is also limited by the maximum doping concentration of activator ions in the matrix lattice. Hence, the upconversion luminescence of samples in this band is generally weak. Therefore, it is crucial that the cross-relaxation and concentration quenching chances induced by high-concentration doping of Er^{3+} ions are attenuated. In this paper, it is found that high-concentration doping of Er^{3+} ions can be realized in the $NaYF_4$ matrix lattice. It is also found that at low-concentration doping, Er^{3+} ions mainly play the role of unsaturated luminescent centers in the lattice. As the doping concentration of Er^{3+} ions continued to increase, firstly, some of the Er^{3+}-2 ions can act as sensitizers to absorb and transfer energy. This causes the remaining Er^{3+}-1 ions to be saturated with excitation so that the upconversion luminescence of the sample is significantly enhanced. Secondly, 1550 nm photons can be well responded by the Ho^{3+} ions in lanthanide activator ions, so mutual sensitization between the Er^{3+} and Ho^{3+} ions can be present. Since the characteristic emissions of Er^{3+} and Ho^{3+} ions are highly overlapping in the visible region, the upconversion luminescence intensity of the sample is significantly enhanced by the additive effect of the two characteristic emissions. At this time, Ho^{3+} ions mainly play the roles of transient energy trapping centers and new luminescence centers in the matrix lattice. On this basis, we also find that the upconversion luminescence intensity of the samples is further enhanced by doping a small amount of Yb^{3+} ions into the above two co-doping systems. At this time, the Yb^{3+} ions mainly play the role of the reverse energy transfer center in the matrix lattice. The energy that should have been dissipated in the supersaturated excitation is stored in the excited state energy level of the Yb^{3+} ions through the energy transfer process. Then, the Er^{3+} ions are secondarily excited by the reverse energy transfer process. Due to this process, the utilization of photons by the sample is drastically increased. As a result, the upconversion luminescence intensity of the triple-doped system is significantly enhanced.

In this paper, upconversion fluoride phosphors $NaY_{1-x-y-z}F_4$:Er_x^{3+}, Ho_y^{3+}, Yb_z^{3+} were synthesized by the low temperature combustion method. The inter-sensitization interaction between Er^{3+}–Ho^{3+}–Yb^{3+} ions was investigated in detail. This study not only provides a new idea for the design of upconversion luminescent materials, but also further improves the energy transfer mechanism between the upconversion multi-doped lanthanide activator and sensitizer ions under 1550 nm excitation.

2. Experimental

2.1 Preparation

The experiments started with sodium fluoride (NaF), rare earth oxides Ln_2O_3 (Ln = Er, Y, Ho and Yb) as raw materials, ammonium hydrogen fluoride (NH_4HF_2), urea [$CO(NH_2)_2$], and ammonium nitrate (NH_4NO_3). The up-conversion fluoride phosphors $NaY_{1-x-y-z}F_4$:Er_x^{3+}, Ho_y^{3+}, Yb_z^{3+} were synthesized by the low-temperature synthesized combustion (LCS) method. First, the rare earth oxides Ln_2O_3 were dissolved in dilute nitric acid to make a solution of rare earth nitrates [$Ln(NO_3)_3$]. The co-precipitation method was adopted to convert rare-earth nitrates into solid rare-earth fluorides (LnF_3). Then the prepared fluoride raw materials were mixed with oxidizer [NH_4NO_3], reductant [$CO(NH_2)_2$] and NH_4HF_2 by adding alcohol to grind them well to obtain prefabricated combustion rods. Finally, they were ignited in a muffle furnace at 650 °C. 10 min later, the crucible was removed, and a fluffy pink powder was obtained. After the samples were cooled, they were gently ground and used for subsequent tests.

2.2 Measurements

The X-ray diffraction (XRD) patterns of the samples were tested with a Rigaku/Ultima IV X-ray diffractometer at 40 kV, 20 mA, with Cu K radiation (λ = 1.5405 Å) and a diffraction angle range of 10 to 80 (2θ). The morphology of the samples was tested using a JSM-6701F scanning electron microscope (SEM) at an accelerating voltage of 10 kV. The upconversion emission spectra of the samples were tested by a Shimadzu RF-5301PC spectrometer and a power-tunable 1550 nm laser at room temperature, the spectrometer's test slit was 1.5 μm and the excitation power was 1.57 mW cm^{-2}.

3. Results and discussion

3.1 Crystal structure analysis

Fig. 1 and 2 show the XRD patterns of the samples doped with different kinds of lanthanides, respectively. Table 1 shows the ionic radius of the lanthanide ions doped in this sample. It is well known that when other lanthanide ions are doped in the matrix

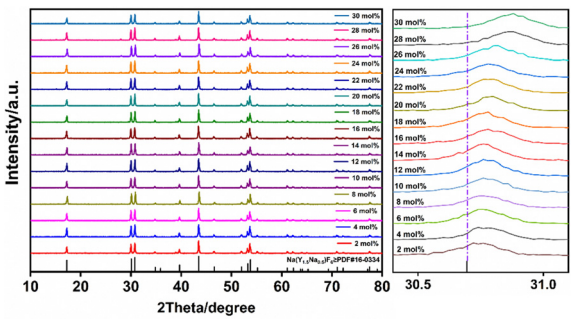

Fig. 1 XRD patterns of doping with different concentrations of Er^{3+} ions.

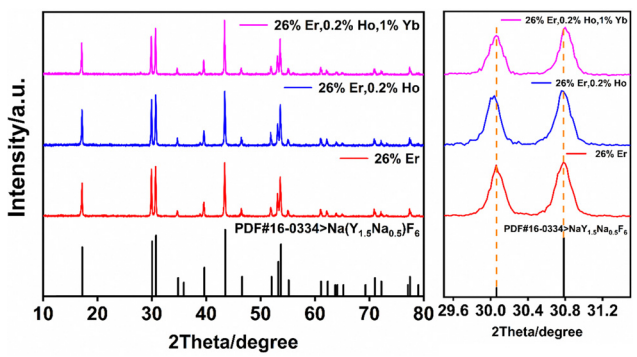

Fig. 2 XRD patterns of samples with different kinds of ion doping.

Table 1 Ionic size of elements

Elements	Y	Er	Ho	Yb
Ionic size [Å]	0.9	0.89	0.901	0.868

lattice, the difference in ion radius will cause the contraction or expansion of the cell of the matrix lattice, thus influencing the sample's up-conversion luminescence characteristics.[9,10] The variation law of the matrix lattice can be described by the interplanar spacing of the hexagonal crystal system and Bragg's law.[11,12]

$$d = \frac{1}{\sqrt{\frac{4}{3}\frac{(h^2+k^2+hk)}{a^2}+\frac{l^2}{c^2}}} \quad (1)$$

$$2d\sin\theta = n\lambda \quad (2)$$

where h, k and l are the crystal indices of the crystal cell, a and c are the prism lengths of the crystal cell, d is the interplanar spacing, θ is the half diffraction angle of the crystal, λ is the excitation wavelength, and n is an integer that indicates the number of diffraction levels of the crystal. Since the phosphor samples are based on $NaYF_4$ doping, the other lanthanide ions have replaced the Y^{3+} ion lattice locations in the matrix lattice. Therefore, when Er^{3+}/Yb^{3+} ions are doped into the units of the matrix lattice, the ionic radii of all these ions are smaller than those of Y^{3+} ions.[13,14] Hence, a certain degree of contraction occurs in the matrix lattice structure. According to eqn (1), h, k and l is constant for a specific family of crystal planes. When the cell parameters become smaller owing to the doping of rare earth ions, the interplanar spacing d decreases accordingly, so the cell's crystal plane spacing decreases. And then, according to eqn (2), when the crystal plane spacing d decreases, the diffraction angle of the sample should be shifted to a large angle direction.[9] This is consistent with the shift of the diffraction peak in the XRD local magnification of Fig. 2. Then, Ho^{3+} ions replace the lattice sites of Y^{3+} ions by doping the matrix lattice, as the radius of these ions is greater than that of Y^{3+} ions.[15] Therefore, according to the above eqn (1) and (2), the XRD diffraction peak of the sample should be shifted in an appropriate angular direction.[10,16] However, due to the minimal doping of Ho^{3+} ions in the sample, the diffraction peak shift of the samples is minimized, which can be further explained by the XRD local magnification pattern in the above figure. Fig. 3 shows a schematic representation of the crystal structure doped with several lanthanide ions. Fig. 4 shows the SEM images of different lanthanide ions doped in the matrix lattice. It is evident from the graph that the majority of grains in the SEM of the sample are hexagonal phase crystals, which is consistent with the crystal phase shown in the XRD standard card of the sample, and the size of the grains mostly remains around 1 μm with a more uniform grain size.

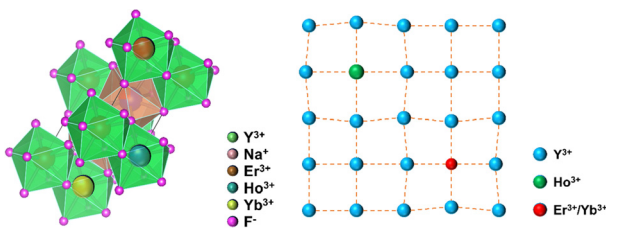

Fig. 3 Schematic diagram of the crystal structure of the sample doped with different types of ions.

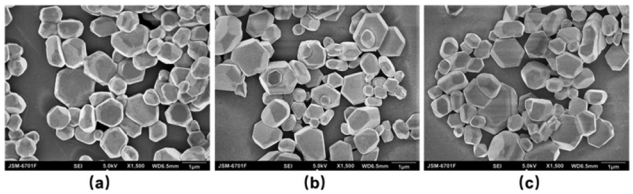

Fig. 4 SEM images of the matrix lattice doped with different kinds of ions: (a) doped Er^{3+} ions, (b) doped Ho^{3+} ions and (c) doped Yb^{3+} ions.

3.2 Modulating effect of the Er^{3+} ion dopant on the upconversion luminescence properties

Er^{3+} ions are often used as activator ions in the 1550 nm band due to their significant absorption of 1550 nm photons.[17,18] Still, they are limited by the cross-relaxation between ions when doped with a high concentration of Er^{3+} ions.[16,19] This has led to the fact that doping with high concentrations of Er^{3+} ions at 1550 nm excitation has been poorly studied.[19] Therefore, the mechanism of the role played by Er^{3+} ions in the upconversion luminescence on the lattice at high doping concentrations is imperfectly studied. Hence, it is necessary to systematically study the mechanism of upconversion luminescence on Er^{3+} ions doped with high concentration.

In this paper, $NaYF_4$:Er^{3+} upconversion fluoride phosphors with different Er^{3+} ion doping concentrations were synthesized by the LCS method. The upconversion emission spectra were determined for different Er^{3+} ion doping concentrations, as shown in Fig. 5 and 6, and a schematic diagram of the energy transfer between Er^{3+} ion single-doped sample ions is also shown. As can be seen from the figure, the doping concentration of Er^{3+} ions gradually increases. The upconversion luminescence intensity of the sample increased first, then decreased, and then increased and then decreased. And thus, two inflection points of high and low upconversion luminescence intensity are generated, which

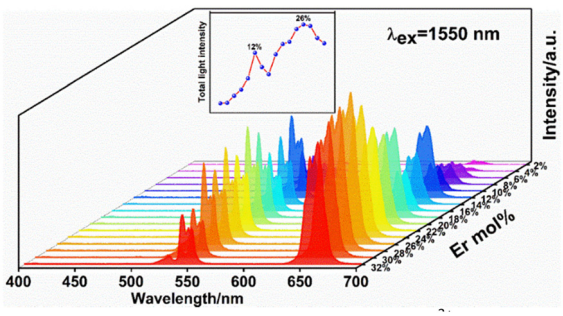

Fig. 5 Upconversion emission spectra from the Er^{3+}-doped samples under 1550 nm excitation.

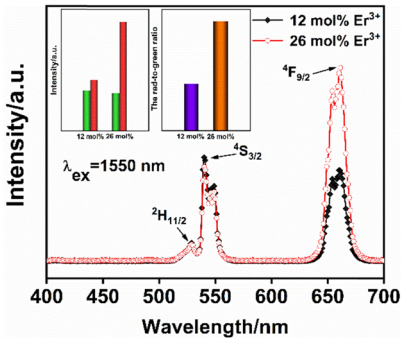

Fig. 6 Emission spectra of Er ions doped with low and high concentration under 1550 nm excitation.

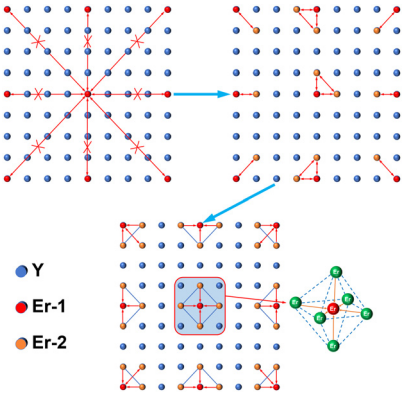

Fig. 7 Schematic diagram of Er^{3+} ion doping energy transfer.

correspond to the doping concentration of Er^{3+} ions of 12 mol% and 26 mol% respectively. The upconversion emission spectrum of the sample consists of 521 nm for green light, 544 nm for red light and 660 nm for red light. For the green emission of the sample, it corresponds to the $^4I_{15/2} \rightarrow {}^2H_{11/2}$ and $^4I_{15/2} \rightarrow {}^4S_{3/2}$ energy level transitions of Er^{3+} ions, and for the red emission of the sample, it corresponds to the $^4I_{15/2} \rightarrow {}^4F_{9/2}$ energy level transitions of Er^{3+} ions. For the red emission of the sample, it corresponds to the energy level transitions of the $^4I_{15/2} \rightarrow {}^4F_{9/2}$ energy levels of Er^{3+} ions. For Er^{3+} ions doped with a high concentration of 26 mol% and low concentration of 12 mol%, the total luminous intensity is increased by 1.62 times, and the red-green ratio is increased by 2.31 times. This is mainly due to the strong response of Er^{3+} ions to 1550 nm photons.[6] The Er^{3+}-1 ions are uniformly distributed in the $NaYF_4$ matrix lattice for the inflection point appearing at low-concentration doping. The probability of the ions undergoing cross-relaxation is small because of the long energy transfer distance between neighboring Er^{3+} ions.[20] In addition, due to the influence of the excitation power, the Er^{3+} ions are in the unsaturated excitation state at this time. With the increase of the Er^{3+} ion doping concentration, the upconversion luminescence intensity of the sample was increased steadily. Afterward, as the doping concentration of Er^{3+} ions continues to be increased, the lattice sites of Y^{3+} ions around the uniformly distributed Er^{3+}-1 ions in the matrix lattice are gradually replaced by Er^{3+}-2 ions. The energy transfer distance between the Er^{3+}-1–Er^{3+}-2 ions is reduced,[21] which results in the probability of cross-relaxation between neighboring ions being dramatically increased. The upconversion luminescence intensity of the sample is gradually reduced because the probability of non-radiative transitions in the sample is increased, and the probability of radiative transitions is decreased. Afterward, the Y^{3+} ion lattice sites around the Er^{3+}-1 ions are gradually and uniformly occupied by more Er^{3+}-2 ions as the Er^{3+} ion doping concentration continues to increase. At this point, the upconversion luminescence intensity of the samples begins to be gradually increased because the energy transfer effect between the Er^{3+}-1–Er^{3+}-2 ions begins to outweigh the cross-relaxation between Er^{3+}-2–Er^{3+}-1 ions. This will make the sample upconversion luminescence intensity begin to increase gradually, so the Er^{3+}-1 ions are gradually saturating excited. When the doping concentration of Er^{3+} ions reaches 26 mol%, the energy transfer between Er^{3+}-2 ions to Er^{3+}-1 ions is greater than the cross-relaxation effect between the ions, reaching the maximum value, and the Er^{3+}-1 ions in the energy receptor exhibit completely saturated excitation. Afterward, as the doping concentration of Er^{3+} ions continues to be increased, the cross-relaxation effect between neighboring ions begins to dominate so that the upconversion luminescence intensity of the sample is gradually reduced.[22–24] This process is shown in Fig. 7.

As shown in Fig. 5, with the gradual increase in the doping concentration of Er^{3+} ions, the red light emission of the single-doped samples with Er^{3+} ions was substantially enhanced, and the green light emission was significantly reduced. Therefore, it is necessary to further analyze the upconversion of red emission and green emission of the samples from the perspective of energy level transition.

Fig. 8(a) shows the energy level transition of Er^{3+} ions under 1550 nm excitation, and Fig. 8(b) shows the IP curve under 1550 nm excitation, from which it can be seen that the energy level transition of Er^{3+} ions under 1550 nm excitation is a three-photon summation process. As for the self-absorption green light emission of Er^{3+} ions, the specific process is that the electrons of Er^{3+} ions in the ground state absorb three photons in succession to transit to the $^2H_{11/2}$ energy level, after which some of the electrons in the $^2H_{11/2}$ energy level directly relax to the ground state and produce green light emission at 525 nm. Secondly, some of the other electrons firstly relax to the $^4S_{3/2}$

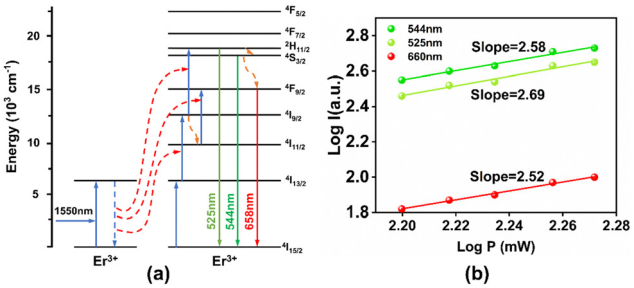

Fig. 8 (a) Energy level transition of Er^{3+} ions under 1550 nm excitation; (b) IP curve of Er^{3+} ions under 1550 nm excitation.

energy level and then return to the ground state by the radiative transition process, producing green light emission of 540 nm.

The reason for the self-absorbed red light emission for Er^{3+} ions is specified as follows. The electrons in the ground state of Er^{3+} ions absorb two photons consecutively to transit to the $^4I_{9/2}$ energy level. Next, these electrons relax to the $^4I_{11/2}$ energy level and then they absorb another photon and transit to the $^4F_{9/2}$ energy level. Finally, these electrons relax to the ground state and produce red light emission at 660 nm. Meanwhile, the electrons of the Er^{3+} ions in the ground state absorb three photons directly to transit to the $^2H_{11/2}$ energy level. Then they first relax to the $^4S_{3/2}$ energy level and then relax to the $^4F_{9/2}$ energy level. They eventually return to the ground state by the radiation transition process and produce the red light emission of the Er^{3+} ions.[6,19,25,26]

In summary, the Er^{3+} ions do not play a single role in the upconversion luminescence of the matrix lattice in the concentration-sequence doping experiments of the Er^{3+} ions. At low-concentration doping, the Er^{3+} ions mainly play the role of the energy acceptor of unsaturated excitation and the luminescence center of the matrix lattice, which leads to the first inflection point of concentration sequence doping. When the doping concentration of Er^{3+} ions is increased, some of the Er^{3+} ions gradually play the roles of energy carriers and energy transfer centers. However, the other part of the Er^{3+} ions play the role of an energy acceptor and saturation excitation center. This creates a second inflection point in the ion concentration doped series of samples. Therefore, we will use the saturation excitation of the Er^{3+} ion concentration as the basis for subsequent studies.

3.3 Modulating effect of the Er^{3+}–Ho^{3+} ion dopant on the upconversion luminescence properties

Currently, studies on the 1550 nm band are mainly focused on the Er^{3+} ion single-doped samples, and there are fewer studies on the response of other ions to the 1550 nm band.[27–29] However, in recent years, it has been found that in the matrix lattice doped with Er^{3+} ions, the upconversion luminescence intensity of the samples can be greatly enhanced by doping with an appropriate amount of other ions.[29,30] In this section, based on the above Er^{3+} ion doping of 26 mol%, the effect of this ion doping on the upconversion luminescence performance of the samples was investigated. As shown in Fig. 9(a), the upconversion luminescence intensity of the samples increased and then decreased when Ho^{3+} ions were doped into the matrix lattice of single-doped Er^{3+} ions. When the doping concentration of Ho^{3+} ions is 0.2 mol%, the upconversion luminescence intensity of the Er^{3+}–Ho^{3+} ion co-doped system reaches the optimum, which is enhanced 1.23 times compared with the undoped Ho^{3+} ion sample, as shown in Fig. 9(b). When the Ho^{3+} ion doping concentration is further increased, the red light emission of the samples gradually dominated, and the green light emission of the samples was significantly quenched. This phenomenon is mainly caused by the different roles played by Ho^{3+} ions in the Er^{3+}–Ho^{3+} co-doped system.

The intrinsic mechanism of upconversion luminescence enhancement and energy transfer is analyzed in more detail. It is first necessary to determine whether the Ho^{3+} ions can act as an independent 1550 nm response upconversion absorption and emission center in the Er^{3+}–Ho^{3+} ion co-doped system. Fig. 10(a) is the upconversion emission spectrum of the Ho^{3+} ion single-doped and Ho^{3+}–Yb^{3+} ion co-doped samples under 1550 nm excitation. Fig. 10(b) shows the absorption spectra of mono-doped with Ho^{3+} ions and mono-doped samples with different concentrations of Er^{3+} ions. As can be seen from the figure, 1550 nm photons are significantly absorbed by the Ho^{3+} ion single-doped samples. The upconversion luminescence of the samples is composed of red and green emission, and the total luminescence intensity is dominated by red emission. For the Ho^{3+}–Yb^{3+} ion co-doped samples, the luminescence of the samples still consists of red and green emission, whereas the total luminescence intensity is still dominated by red emission. Both the red and green light emission of the sample is reduced by doping with Yb^{3+} ions compared to the single-doped samples with Ho^{3+} ions. However, since there are almost no studies on the 1550 nm band that can be well responded to by other lanthanide activator ions, the current mechanism of upconversion energy level transition of Ho^{3+} ions under 1550 nm excitation is not well developed. In this section, the energy of each spectral term of Ho^{3+} ions was determined by reviewing the relevant literature, as shown in Table 2. After that, the energy difference between each spectral term was calculated: $\Delta E_1 = 5049\ cm^{-1}$ ($^5I_8 \rightarrow {}^5I_7$), $\Delta E_2 = 6061\ cm^{-1}$ ($^5I_7 \rightarrow {}^5I_5$), $\Delta E_3 = 4264\ cm^{-1}$ ($^5F_5 \rightarrow {}^5I_5$), $\Delta E_4 = 5289\ cm^{-1}$ ($^5F_4 \rightarrow {}^5I_4$).[31] By comparing with the energy carried by 1550 nm photons ($\Delta E_{1550\ nm} = 6452\ cm^{-1}$) and combining with the IP curves of 1550 nm excitation of single-doped Ho^{3+} ions, as shown in Fig. 11(a), the upconversion energy level transition

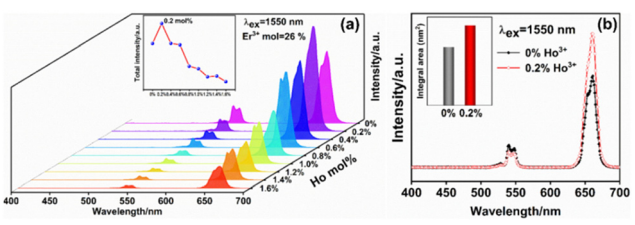

Fig. 9 (a) Upconversion emission spectra of Er^{3+}–Ho^{3+} co-doped samples under 1550 nm excitation. (b) Upconversion emission spectra of the optimally doped sample with Ho^{3+} ions and undoped sample with Ho^{3+} ions.

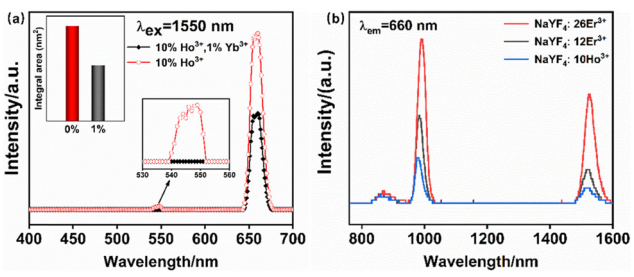

Fig. 10 (a) Upconversion emission spectra of the single-doped sample with Ho^{3+} ions and co-doped sample with Ho^{3+}–Yb^{3+} under 1550 nm excitation. (b) Absorption spectra of the samples singly doped with Ho^{3+} ions and singly doped with Er^{3+} ions.

Table 2 Energy difference of each spectral term for Ho^{3+} ions

Energy level	$^5I_7$	$^5I_6$	$^5I_5$	$^5I_4$	$^5F_5$	$^5S_2$	$^5F_4$
ΔE (cm^{-1})	5049	8550	11 110	13 155	15 374	18 325	18 444

diagrams of the Ho^{3+} ions excited at 1550 nm were determined, as shown in Fig. 11(b). The absorption of 1550 nm photons by Ho^{3+} ions makes Ho^{3+} ions play more roles in the Er^{3+}–Ho^{3+} ion co-doping system. Firstly Ho^{3+} ions can be self-absorbing emission centers in the matrix lattice. Since the characteristic emissions of Er^{3+} ions and Ho^{3+} ions are highly overlapped in the visible region,[29] the upconversion emission spectra of Er^{3+}–Ho^{3+} ion co-doped samples are generated by the superposition of the characteristic emissions of both, which enhances the upconversion luminescence of the samples.[29] Secondly, Ho^{3+} ions can also act as a reverse energy transfer center in the matrix lattice. The photon energy absorbed by the Er^{3+} ions is first temporarily stored by the Ho^{3+} ions. Then, the energy is transferred back to the Er^{3+} ions again by the reverse energy transfer process. Through this process, some of the Er^{3+} ions are excited twice, and the upconversion luminescence of the sample is enhanced.[28,32] Finally, the Ho^{3+} ions can also act as an energy receptor for the Er^{3+} ions. The energy transferred from the Er^{3+} ions is absorbed by these Ho^{3+} ions and produces their characteristic emission, causing the upconversion luminescence of the Er^{3+}–Ho^{3+} ion co-doped sample to be to enhanced.

In summary, combining the upconversion emission spectra of the samples of the Er^{3+}–Ho^{3+} ion co-doped system, it can be seen that the addition of the green emission of Er^{3+} ions and Ho^{3+} ions in the visible region produces the upconversion green emission of the samples. Fig. 12(a) shows the energy level transition of the Er^{3+}–Ho^{3+} ion co-doped sample under 1550 nm excitation, and Fig. 12(b) shows the IP curve of the Er^{3+}–Ho^{3+} ion co-doped sample under 1550 nm excitation. It can be seen that the energy level transition of the Er^{3+}–Ho^{3+} ion co-doping system under 1550 nm excitation is a three-photon summation process. For the green emission of Er^{3+} ions of the samples, due to the doping of Ho^{3+} ions, the green emission pathway of Er^{3+} ions is increased by the reverse energy transfer process between Er^{3+}–Ho^{3+} ions. The process is that the electrons of the Er^{3+} ions in the $^4S_{3/2}$ energy level transfer to the neighboring Ho^{3+} ions by the energy transfer process. Then, these electrons are stored on the $^5F_4$ energy level of the Ho^{3+} ions,

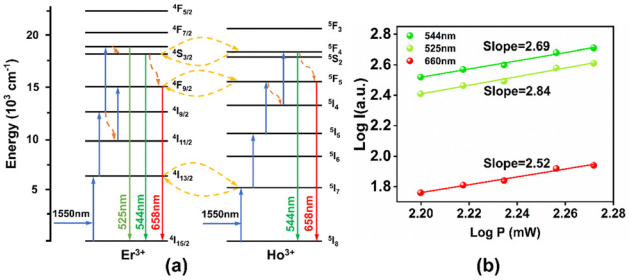

Fig. 12 (a) Energy level transition of Er^{3+}–Ho^{3+} ions co-doped under 1550 nm excitation. (b) IP curve of Er^{3+}–Ho^{3+} ions co-doped under 1550 nm excitation.

after which they return to the $^4S_{3/2}$ energy level of the Er^{3+} ions by the reverse energy transfer process. Finally, these electrons relax to the ground state and produce green light at 544 nm.[28,29,33]

As for the upconversion green light emission of Ho^{3+} ions, it mainly consists of three parts, the first part is the self-absorption green light emission of Ho^{3+} ions, and the second part is the green light emission generated by the reverse energy transfer process between Ho^{3+}–Er^{3+} ions. The third is the green light emission generated by the energy transfer process between Er^{3+}–Ho^{3+}.

For the self-absorbed green light emission of Ho^{3+} ions, the main process is that the electrons of the Ho^{3+} ions in the ground state absorb three photons consecutively to transit to the $^5F_5$ energy level, after which they relax to the $^5I_4$ energy level. Then these electrons absorb another photon to transit to the $^5F_4$ energy level. Finally, they return to the ground state by a radiative transition process and produce the green light emission of the Ho^{3+} ions at 544 nm, and this process is shown in Fig. 13(a).

For the green light emission of the Ho^{3+} ions generated by the reverse energy transfer process between Ho^{3+}–Er^{3+}, the specific process is that the electrons in the $^5F_5$ energy level of the Ho^{3+} ions transfer to the $^4F_{9/2}$ energy level of the neighboring Er^{3+} ions by an energy transfer process. These electrons return to the $^5F_5$ energy level of the Ho^{3+} ions by the reverse energy transfer process and further relax to the $^5I_4$ energy level. Next these electrons absorb a photon to transit to the $^5F_4$ energy level. Finally, they return to the ground state by the radiative transition process and produce green light emission of the Ho^{3+} ions. On the other hand, the electrons in the $^5F_4$ energy level of the Ho^{3+} ions can also be transferred to the $^4S_{3/2}$ energy level of the

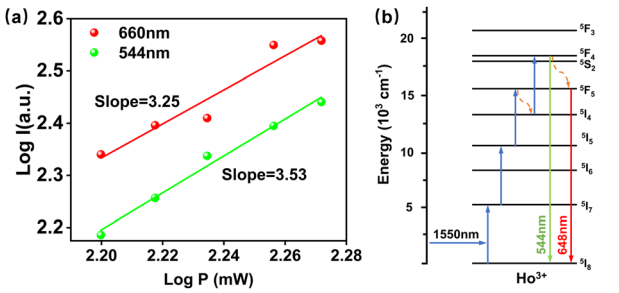

Fig. 11 (a) IP curves of singly doped samples with Ho^{3+} ions under 1550 nm excitation. (b) Upconversion energy level transition diagram of Ho^{3+} ions under 1550 nm excitation.

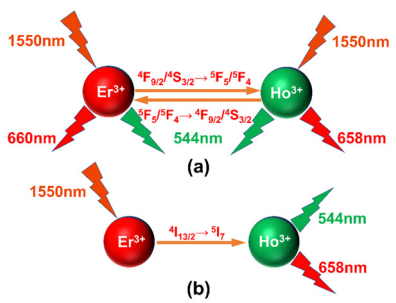

Fig. 13 (a) Schematic diagram of the reverse energy transfer of Er^{3+}–Ho^{3+} ions. (b) Schematic diagram of the energy transfer of Er^{3+}–Ho^{3+} ions.

neighboring Er^{3+} ions through an energy transfer process and return to the $^5F_4$ energy level of the Ho^{3+} ions by the reverse energy transfer process. They eventually relax to the ground state and produce green light emission of the Ho^{3+} ions, and this process is shown in Fig. 13(a).[28,29]

The reason for the green light emission generated by the energy transfer process between Er^{3+}–Ho^{3+} ions is specified as follows, the electrons in the $^4I_{13/2}$ energy level of Er^{3+} ions transfer to the neighboring Ho^{3+} ions by the energy transfer process, keeping these electrons in the $^5I_7$ energy level of Ho^{3+} ions. Meanwhile, the electrons at the $^5I_7$ energy level absorb two photons consecutively to transit to the $^5F_5$ energy level, and they relax to the $^5I_4$ energy level. And then, these electrons absorb a photon to transit to the $^5F_4$ energy level. Finally, they return to the ground state by the radiative transition process and produce green light emission of Ho^{3+} ions, and this process is shown in Fig. 13(b).[28,29,34]

For the Er^{3+}–Ho^{3+} ion co-doped system under 1550 nm excitation, the red light emission is also generated by summating the red light emission of Er^{3+} ions and the Ho^{3+} ions in the visible region. For the red emission of Er^{3+} ions of the samples, due to the doping of Ho^{3+} ions, the red emission pathway of Er^{3+} ions is increased by the reverse energy transfer process between Er^{3+}–Ho^{3+} ions. The specific process is that the electrons of the Er^{3+} ions in the $^4S_{3/2}$ energy level transfer to the neighboring Ho^{3+} ions by the energy transfer process, and these electrons return to the $^4S_{3/2}$ energy level of the Er^{3+} ions by the reverse energy transfer process. Then these electrons relax to the $^4F_{9/2}$ energy level. Finally, they return to the ground state by the radiative transition process and produce red light emission of the Er^{3+} ions. On the other hand, the electrons in the $^4F_{9/2}$ energy level of the Er^{3+} ions can also transfer to the $^5F_5$ energy level of the neighboring Ho^{3+} ions by the energy transfer process, and these electrons return to the $^4F_{9/2}$ energy level by the reverse energy transfer process. Finally, they relax to the ground state and produce the red light emission of the Er^{3+} ions, and this process is shown in Fig. 13(a).[28,29,35]

As for the upconversion red light emission of Ho^{3+} ions, it mainly consists of three parts, the first is the self-absorption red light emission of Ho^{3+} ions, and the second is the red light emission generated by the reverse energy transfer process between Ho^{3+}–Er^{3+} ions. The third is the red light emission generated by the energy transfer process between Er^{3+}–Ho^{3+} ions.

For the self-absorbed red light emission of Ho^{3+} ions, the main process is that the electrons of the Ho^{3+} ions in the ground state absorb three photons consecutively to transit to the $^5F_5$ energy level. Then they immediately relax to the ground state and produce the red light emission of the Ho^{3+} ions. On the other hand, the electrons of the Ho^{3+} ions in the $^5F_5$ energy level relax to the $^5I_4$ energy level, and absorb another photon to transit to the $^5F_4$ energy level. Finally, they return to the ground state by a radiative transition process and produce the red light emission of the Ho^{3+} ions.

For the red light emission of the Ho^{3+} ions generated by the reverse energy transfer process between Ho^{3+}–Er^{3+}, the specific process is that the electrons in the $^5F_5$ energy level of the Ho^{3+} ions can transfer to the $^4F_{9/2}$ energy level of the neighboring Er^{3+} ions by an energy transfer process. After that, these electrons return to the $^5F_5$ energy level of the Ho^{3+} ions by the reverse energy transfer process. Then, they return to the ground state by the radiative transition process and produce red light emission of the Ho^{3+} ions, and this process is shown in Fig. 13(a).[28,29,35]

The reason for the red light emission generated by the energy transfer process between Er^{3+}–Ho^{3+} ions is specified as follows. The electrons in the $^4I_{13/2}$ energy level of Er^{3+} ions transfer to the neighboring Ho^{3+} ions by the energy transfer process, keeping these electrons in the $^5I_7$ energy level of Ho^{3+} ions. Then, these electrons at the $^5I_7$ energy level absorb two photons consecutively to transit to the $^5F_5$ energy level. They relax to the ground state and produce red light emission of Ho^{3+} ions. On the other hand, the electrons of the Er^{3+} ions in the $^4F_{9/2}$ energy level transfer to the $^5F_5$ energy level of the neighboring Ho^{3+} ions by an energy transfer process, and then they return to the ground state by a radiative transition process and produce the red light emission of the Ho^{3+} ions; this process is shown Fig. 13(b).[28,29,35]

Fig. 14 shows the fluorescence lifetime decay curves of the Er^{3+}–Ho^{3+} ion co-doped samples under 980 nm excitation. The graph shows that the co-doped Er^{3+}–Ho^{3+} will lead to a certain degree of enhancing the fluorescence lifetime of 540 nm. This is mainly due to the doping of Ho^{3+} ions, which makes the electrons on the $^2H_{11/2}$ and $^4S_{3/2}$ energy levels of the Er^{3+} ions sustain a longer period. This decreases the chance of electrons at this energy level returning to the ground state. Therefore, the fluorescence weakening of 540 nm will appear in the upconversion emission spectrum. On the contrary, doping the Er^{3+} ions with the appropriate amount of Ho^{3+} ions will result in a substantial enhancement of the red emission of the samples. And the fluorescence lifetime of 660 nm is reduced after being doped with Ho^{3+} ions. This is mainly due to many electrons preferentially returning to the ground state and producing the red light emission of 660 nm. Therefore, all these factors increase the red lifetime of Er^{3+}–Ho^{3+} ion co-doped samples. The reduction of 660 nm lifetime also corroborates the significant enhancement of the red emission presented by the emission spectrum.[36]

The fluorescence decay curves are experimental evidence of energy transfer between rare earths. In order to further clarify the energy transfer mechanism of Ho^{3+} ion doping, we calculated the energy transfer efficiency of Er^{3+} ions co-doped with Er–Ho samples as shown in eqn (3):

$$\eta_{ET} = 1 - \frac{\tau_{Er-Ho}}{\tau_{Er}} \quad (3)$$

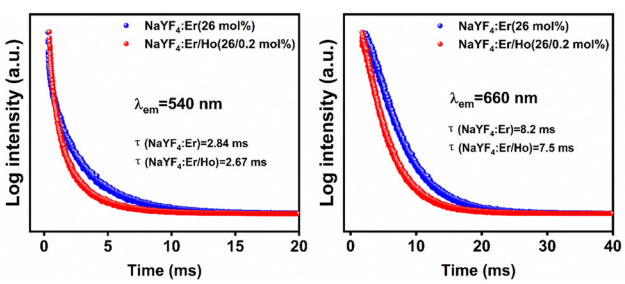

Fig. 14 Fluorescence lifetime of the sample when excited in the 980 nm band.

where τ_{Er-Ho} is the fluorescence lifetime of Er^{3+} ions in the Er^{3+}–Ho^{3+} co-doped sample, and τ_{Er} is the fluorescence lifetime of Er^{3+} ions in the Er ion mono-doped sample. From the above equations and combining the fluorescence lifetimes of the Er^{3+} ion mono-doped with the Er^{3+}–Ho^{3+} co-doped at 540 nm and 660 nm, it can be seen that the energy transfer efficiency of the sample is in the range of 5.99–8.53%. The above results indicate that there is a cross-relaxation process between Er^{3+} ions and Ho^{3+} ions, which leads to a positive trend in the population size. This leads to a positive trend in population accumulation at the $^4F_{9/2}$ energy level of the Er^{3+} ions, which promotes the emission of the sample at 660 nm.

Since in the Er^{3+}–Ho^{3+} ion co-doped system, the doping amount of Ho^{3+} ions is extremely small compared to the optimal doping concentration of Er^{3+} ions, the contribution of the characteristic emission of Ho^{3+} ions to the upconversion luminescence of the sample is extremely weak. Therefore, the upconversion luminescence of the sample is still dominated by the luminescence of Er^{3+} ions. As compared to the increase in the green emission pathway of the Er^{3+}–Ho^{3+} ion co-doped sample, the red light emission pathway is significantly more than the green light emission. Due to the combined effect of cross-relaxation and energy transfer between the ions, the chance of the electron population to the green light energy level is greatly reduced. So the green light emission of the Er^{3+}–Ho^{3+} co-doped samples is significantly quenched, while the red light emission is substantially enhanced.

3.4 Modulating the effect of Er^{3+}–Ho^{3+}–Yb^{3+} ion dopants on the upconversion luminescence properties

In the above study, the role played by Ho^{3+} ions in the Er^{3+}–Ho^{3+} co-doping system and the enhancement of upconversion luminescence was investigated. Afterward, it was found that the upconversion luminescence of the samples doped with Er^{3+} ions was significantly enhanced after doping with Yb^{3+} ions. Combined with the above Ho^{3+}–Yb^{3+} ion co-doping experiment, the doping of Yb^{3+} ions can make the Ho^{3+} ions continue to produce the characteristic red and green light emission, but the upconversion luminescence of Ho^{3+} ions is reduced under the excitation at 1550 nm. This may be due to the large energy difference between the $^2F_{5/2}$ energy level of the Yb^{3+} ion and the $^5I_6$ energy level of the Ho^{3+} ions.[37] The reverse energy transfer process between the Ho^{3+}–Yb^{3+} ion was difficult to occur. Therefore, the doping of Yb^{3+} ions depletes the energy absorbed by Ho^{3+} ions, the upconversion luminescence intensity of the Ho^{3+}–Yb^{3+} co-doped system was reduced. Consequently, in this section, the appropriate amount of Yb^{3+} ions based on the optimal doping concentration of Er^{3+}–Ho^{3+} ions mentioned above was doped, and the role of Yb^{3+} ions in the multi-ion co-doped system and the effect on the upconversion luminescence performance of the samples was investigated.

Fig. 15 shows the upconversion emission spectra of the Er^{3+}–Ho^{3+}–Yb^{3+} ion triple-doped samples under 1550 nm excitation. As can be seen from the figure, as the doping concentration of Yb^{3+} ions was increased, the upconversion luminescence intensity of the samples increases firstly and then decreases. When

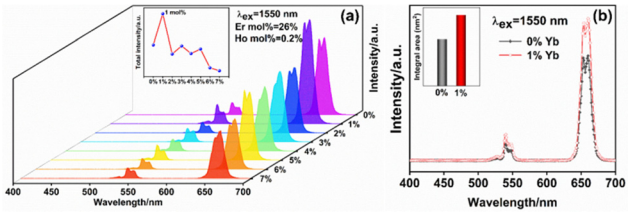

Fig. 15 (a) Upconversion emission spectra of Er^{3+}–Ho^{3+}–Yb^{3+}triple-doped samples under 1550 nm excitation. (b) Upconversion emission spectra of the optimally doped sample with Yb^{3+} ions and the undoped sample with Yb^{3+} ions.

the Yb^{3+} ion doping concentration is 1 mol%, the upconversion luminescence intensity of the sample reaches the best value. The red and green emission intensities of the samples are enhanced to a certain extent after the doping of Yb^{3+} ions in the matrix lattice. Since the photons of 1550 nm are not absorbed by Yb^{3+} ions, the photons in the Er^{3+}–Ho^{3+}–Yb^{3+} ion doped samples are mainly accomplished by Er^{3+} ions, and a small portion of the photons are absorbed by Ho^{3+} ions.[29,30] By reviewing the relevant literature and combining the experimental phenomena, it can be seen that Yb^{3+} ions for the Er^{3+}–Ho^{3+}–Yb^{3+} triple-doped system of upconversion luminescence mainly plays the role of a reverse energy transfer center of Er^{3+}–Yb^{3+} ions. This process means that the utilization rate of the Er^{3+} ions for the photons is increased so that the intensity of the upconversion luminescence is significantly increased. The energy transfer between the Ho^{3+}–Yb^{3+} ions leads to rapid energy depletion, so the upconversion luminescence intensity of the Ho^{3+}–Yb^{3+} co-doped samples is significantly quenched.

Fig. 16(a) shows the energy level transition of the Er^{3+}–Ho^{3+}–Yb^{3+}ion triple-doped sample under 1550 nm excitation, and Fig. 16(b) shows the IP curve of the Er^{3+}–Ho^{3+}–Yb^{3+}ion triple-doped sample under 1550 nm excitation, from which it can be seen that the energy level transition of the Er^{3+}–Ho^{3+}–Yb^{3+}ion triple-doped system under 1550 nm excitation is a three-photon summation process. For the Er^{3+}–Ho^{3+}–Yb^{3+} triple-doped system under 1550 nm excitation, the increased green emission pathway due to the doping of Yb^{3+} ions mainly consists of the green emission of Er^{3+} ions. The specific process is that the electrons of the Er^{3+} ions in the ground state absorb two photons in succession to transit to the $^4I_{9/2}$ energy level, after

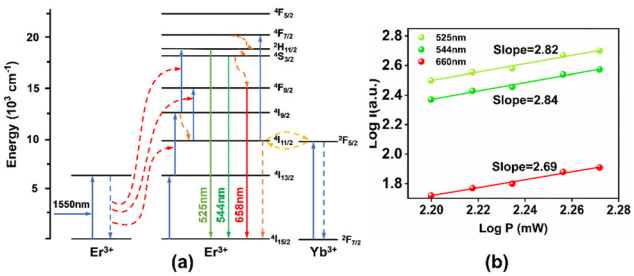

Fig. 16 (a) Energy level transition of Er^{3+}–Ho^{3+}–Yb^{3+}ion triple-doping under 1550 nm excitation. (b) IP curve of Er^{3+}–Ho^{3+}–Yb^{3+}ion triple-doping under 1550 nm excitation.

which they relax to the $^4I_{11/2}$ energy level. Then, these electrons transfer to the neighboring Yb^{3+} ions by the energy transfer process and keep the electrons in the $^2F_{5/2}$ energy level of the Yb^{3+} ions. And then, these electrons return to the neighboring Er^{3+} ions by a reverse energy transfer process, making the electrons in the $^4I_{11/2}$ energy level directly transit to the $^4F_{7/2}$ energy level, after which these electrons relax to the $^2H_{11/2}$ energy level and the $^4S_{3/2}$ energy level. Finally, they return to the ground state by the radiative transfer process and produce green light emission of the Er^{3+} ions.[38–40]

For 1550 nm excitation in the Er^{3+}–Ho^{3+}–Yb^{3+} triple-doped system, the red light emission pathway is increased due to the doping of Yb^{3+} ions. This mainly originates from the reverse energy transfer process of Er^{3+}–Yb^{3+} ions. The specific process is that the electrons of the Er^{3+} ions in the ground state continuously absorb two photons to transit to the $^4I_{9/2}$ energy level, and then they relax to the $^4I_{11/2}$ energy level. Then these electrons are transferred to the $^2F_{5/2}$ energy level of the neighboring Yb^{3+} ions by the energy transfer process, and afterward they return to the $^4I_{11/2}$ energy level of the Er^{3+} ions by the reverse energy transfer process. These electrons absorb a photon to transit to the $^4F_{9/2}$ energy level, and they eventually return to the ground state by the radiation transition process and produce red light emission of the Er^{3+} ions. Finally, the electrons at the $^2H_{11/2}$ energy level with the electrons on the $^4I_{11/2}$ energy level of the Er^{3+} ions can undergo a cross-relaxation process, making the electrons at the $^4I_{11/2}$ energy level transit to the $^4F_{9/2}$ energy level, after which these electrons return to the ground state by the radiation transition process and produce the red light emission of the Er^{3+} ions.[36,41–43] Fig. 17 shows the schematic diagram of the reverse energy transfer between Yb^{3+} ions and Er^{3+} ions and Ho^{3+} ions. Through the above experimental results, we only observed the reverse energy transfer process between Er^{3+}–Yb^{3+} ions; the reverse energy transfer phenomenon between Ho^{3+}–Yb^{3+} ions did not occur. Therefore, for the Er^{3+}–Yb^{3+} ion pair, the up-conversion luminescence intensity of the sample is significantly enhanced because the process can significantly increase the utilization rate of Er^{3+} ions for 1550 nm photons.[44–53] Since we do not observe the reverse energy transfer between Ho^{3+}–Yb^{3+} ion pairs, the up-conversion luminescence intensity of the samples was significantly quenched due to the cross-relaxation between the Ho^{3+}–Yb^{3+} ions. The schematic diagram of the reverse energy transfer between the ions in Fig. 17 can well summarize the process of the reverse energy transfer between the Er^{3+}–Ho^{3+}–Yb^{3+} ions.

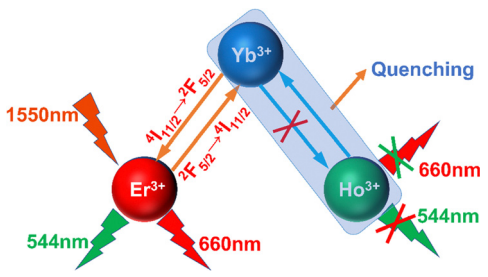

Fig. 17 Schematic diagram of reverse energy transfer of Er^{3+}–Yb^{3+} ions.

In summary, for the upconversion luminescence of the Er^{3+}–Ho^{3+}–Yb^{3+} multi-ion co-sensitized samples, the upconversion red and green emissions of the samples are generated by the summation of the characteristic emissions of the Er^{3+} ions and Ho^{3+} ions in the visible region. Since the doping concentration of Er^{3+} ions is much larger than that of Ho^{3+} ions, the contribution to the upconversion luminescence intensity of the triple-doped Er^{3+}–Ho^{3+}–Yb^{3+} system is still dominated by Er^{3+} ions. The Ho^{3+} ions play the energy transfer capture center role in the upconversion luminescence of the samples. Meanwhile, they may also be part of the self-absorption activation center and the energy receptor luminescence center of the Er^{3+} ions. The doping of Yb^{3+} ions mainly plays the role of the reverse energy transfer center between Er^{3+}–Yb^{3+} ion pairs. Although the doping of Yb^{3+} ions in the Ho^{3+}–Yb^{3+} co-doped samples significantly reduces the up-conversion luminescence intensity of the samples, the doping concentration of Ho^{3+} ions in the Er^{3+}–Ho^{3+}–Yb^{3+} triple-doped system is very small. Therefore, Yb^{3+} ions have little effect on the characteristic emission of Ho^{3+} ions in the triple-doped samples. Meanwhile, Ho^{3+} ions and Yb^{3+} ions can act as energy transient capture centers and reverse energy transfer centers in the matrix lattice structure, respectively. And the energy that should be dissipated in the energy transfer and electron transition process will be stored temporarily, which increases the ions' utilization rate for photons. Absorption of 1550 nm photons by Ho^{3+} ions results in spectral addition. In summary, these factors can enhance the upconversion emission spectral intensity of the samples.

4. Conclusions

Er^{3+}–Ho^{3+}–Yb^{3+} triple-doped fluoride up-conversion phosphors were successfully prepared by the low-temperature combustion synthesis method. It is found that in the series of doping concentrations of Er^{3+} ions under 1550 nm excitation, when the doping concentration of Er^{3+} ions is 12 mol%, due to the limitation of excitation power, Er^{3+}-1 ions mainly play the role of unsaturated excitation centers in the matrix lattice. When the doping concentration of Er^{3+} ions continues to increase until it reaches 26 mol%, Er^{3+}-2 ions will be uniformly distributed around the Er^{3+}-1 ions, playing the role of a sensitizer in the matrix lattice, and saturation excitation of the Er^{3+}-1 ions will significantly enhance the upconversion of the luminescence intensity. The upconversion luminescence intensity of the Er^{3+}–Ho^{3+} co-doped samples is enhanced when a small amount of Ho^{3+} ions are doped into the matrix lattice. The upconversion luminescence intensity of the samples reaches the optimal value when the doping concentration of Ho^{3+} ions is 0.2 mol%, and the doping of Ho^{3+} ions substantially enhances the red emission of the samples and bursts the green light emission. At this time, Ho^{3+} ions can firstly play the roles of transient energy capture centers and reverse energy transfer centers in the matrix lattice, and secondly also act as the self-absorption luminescence center in the matrix lattice. The upconversion luminescence intensity of the Er^{3+}–Ho^{3+}–Yb^{3+} triple-doped system reaches the optimal value when 1 mol% of Yb^{3+} ions is doped in the Er^{3+}–Ho^{3+} co-doped sample. At this time, Yb^{3+} ions

mainly play the role of the reverse energy transfer center between Er^{3+}–Yb^{3+} ion pairs in the matrix lattice. This study has significant applications in enhancing the upconversion luminescence of the samples and displaying high color purity in the 1550 nm band.

Author contributions

Bohan Lei: conceptualization, data curation, formal analysis, investigation, writing original draft. Liping Lu: supervision, writing – review & editing. Haiying Sun: formal analysis, investigation.

Conflicts of interest

There are no conflicts of interest to declare.

Acknowledgements

This work was supported by the Application Innovation Program of the Equipment pre-research (627011103) and the Jilin Province Education Department Project (grant no. JJKH20200760KJ).

Notes and references

1 X. Zhu, Q. Su and W. Feng, *et al.*, Anti-Stokes shift luminescent materials for bio-applications, *Chem. Soc. Rev.*, 2017, **46**(4), 1025–1039.
2 N. Li, N. Eedugurala and D. S. Leem, *et al.*, Organic upconversion imager with dual electronic and optical readouts for shortwave infrared light detection, *Adv. Funct. Mater.*, 2021, **31**(16), 2100565.
3 L. Gao, X. Shan and X. Xu, *et al.*, Correction: Video-rate upconversion display from optimized lanthanide ion doped upconversion nanoparticles, *Nanoscale*, 2020, **12**(36), 18987.
4 F. Jia, G. Li and B. Yang, *et al.*, Investigation of rare earth upconversion fluorescent nanoparticles in biomedical field, *Nanotechnol. Rev.*, 2019, **8**(1), 1–17.
5 W. Wang, J. Tian and J. Dong, *et al.*, Growth, spectroscopic properties and up-conversion of Yb, Pr co-doped CaF_2 crystals, *J. Lumin.*, 2021, **233**, 117931.
6 H. N. Luitel, S. Mizuno and Y. Takeda, $CaTiO_3$:Er^{3+}, Ni^{2+} broadband-sensitive upconverter: an effective way to harvest unused NIR solar irradiation for crystalline silicon solar cells, *Phys. Status Solidi A*, 2017, **214**(8), 1600899.
7 Z. Li, H. Yuan and W. Yuan, *et al.*, Upconversion nanoprobes for biodetections, *Coord. Chem. Rev.*, 2018, **354**, 155–168.
8 X. Yin, W. Hong and X. Mingming, *et al.*, Upconversion luminescence of $Y_2Ti_2O_7$:Er^{3+} under 1550 and 980 nm excitation, *J. Rare Earths*, 2017, **35**(3), 230–234.
9 N. Y. Mostafa, A. Badawi and S. I. Ahmed, Influence of Cu and Ag doping on structure and optical properties of In_2O_3 thin film prepared by spray pyrolysis, *Results Phys.*, 2018, **10**, 126–131.
10 H. Bian, Y. Liu and D. Yan, *et al.*, Light-induced electrons suppressed by Eu^{3+} ions doped in $Ca_{11.94-x}Sr_xAl_{14}O_{33}$ caged phosphors for LED and FEDs, *J. Am. Ceram. Soc.*, 2017, **100**(8), 3467–3477.
11 C. G. Pope, X-ray diffraction and the Bragg equation, *J. Chem. Educ.*, 1997, **74**(1), 129.
12 Y. Liu, Y. Liu and M. G. B. Drew, Comparison of calculations for interplanar distances in a crystal lattice, *Crystallogr. Rev.*, 2017, **23**(4), 252–301.
13 K. N. Nicholson and S. A. Wood, Aqueous Geochemistry of Rare Earth Elements and Yttrium. XII: Potentiometric Stability Constant Determination of Bis -Tris Complexes with La, Nd, Eu, Gd, Yb, Dy, Er, Lu, and Y, *J. Solution Chem.*, 2002, **31**(9), 703–717.
14 S.-O. Yoon, C.-B. Hong and S. Kim, Microwave dielectric properties of Na^+ and M^{3+}-doped $Ba(Mg_{0.5}W_{0.5})O_3$ ceramics, *J. Electroceram.*, 2018, **41**, 16–22.
15 A. Ghafoor, M. A. Khan and M. U. Islam, *et al.*, Structural and electromagnetic studies of $Ni_{0.7}Zn_{0.3}Ho_{2x}Fe_{2-2x}O_4$ ferrites, *Ceram. Int.*, 2016, **42**(12), 14252–14256.
16 W. S. Silveira and A. J. S. Silva, Nascimento P a M D, *et al.* Improving the luminescence properties of YAG:Ce^{3+} phosphors by co-doping Sr^{2+} ions, *Optik*, 2021, **231**, 166363.
17 Y. Chen, F. Peng and Q. Zhang, *et al.*, Growth, structure and spectroscopic properties of 1 at% Er^{3+}:$GdTaO_4$ laser crystal, *J. Lumin.*, 2017, **192**, 555–561.
18 M. Li, S. Sun and L. Zhang, *et al.*, Growth and spectral properties of a promising laser crystal Yb^{3+}/Er^{3+}:$Ca_9La(VO_4)_7$, *J. Cryst. Growth*, 2016, **451**, 52–56.
19 C. Xu, Q. Yang and G. Ren, *et al.*, Pure red upconversion emission from $Yb_3Al_5O_{12}$ phase doped with high Er^{3+} concentration, *J. Alloys Compd.*, 2010, **503**(1), 82–85.
20 H. Krzyżanowska, Y. Fu and K. S. Ni, *et al.*, Efficient Energy Transfer between Si Nanostructures and Er Located at a Controlled Distance, *ACS Photonics*, 2016, **3**(4), 564–570.
21 N. V. Kononets, V. V. Seminko and P. O. Maksimchuk, *et al.*, Processes of energy migration in mixed europium–lanthanum magnesium borate nanocrystals, *Spectrosc. Lett.*, 2017, **50**(7), 399–403.
22 H. Hanchang, Z. Yanyi and L. Mingchen, *et al.*, The effect of Er^{3+} concentration on the kinetics of multiband upconversion in $NaYF_4$:Yb/Er microcrystals, *Front. Chem.*, 2023, **11**, 1097250.
23 L. Yan, B. Zhou and N. Song, *et al.*, Self-sensitization induced upconversion of Er^{3+} in core–shell nanoparticles, *Nanoscale*, 2018, **10**(37), 17949–17957.
24 C. Lee, *et al.*, Origin of strong red emission in Er^{3+}-based upconversion materials: role of intermediate states and cross relaxation, *Phys. Chem. Chem. Phys.*, 2019, **21**(43), 24026–24033.
25 A. R. Hong, J.-H. Kyhm and G. Kang, *et al.*, Orthogonal R/G/B Upconversion Luminescence-based Full-Color Tunable Upconversion Nanophosphors for Transparent Displays, *Nano Lett.*, 2021, **21**(11), 4838–4844.
26 G. A. Kumar, M. Pokhrel and D. K. Sardar, Intense visible and near infrared upconversion in M_2O_2S:Er (M = Y, Gd, La) phosphor under 1550 nm excitation, *Mater. Lett.*, 2012, **68**, 395–398.
27 W. Wang, Z. Feng and B. Li, *et al.*, Er^{3+} self-sensitized nanoprobes with enhanced 1525 nm downshifting emission for NIR-IIb *in vivo* bio-imaging, *J. Mater. Chem. B*, 2021, **9**(12), 2899–2908.

28 Y. Bowen, G. Linna and L. Tiesheng, Nearly pure red up-conversion emission of $Ba_4Bi_3F_{17}$:Ln^{3+} with 1550 nm wavelength excitation by controlling the doping ions, *Opt. Mater.*, 2022, **125**, 112076.
29 X. Cheng, H. Ge and Y. Wei, *et al.*, Design for Brighter Photon Upconversion Emissions *via* Energy Level Overlap of Lanthanide Ions, *ACS Nano*, 2018, **12**(11), 10992–10999.
30 X. Cheng, Y. Pan and Z. Yuan, *et al.*, Er^{3+} Sensitized Photon Upconversion Nanocrystals, *Adv. Funct. Mater.*, 2018, **28**(22), 1800208.
31 A. Y. Freidzon, I. A. Kurbatov and V. I. Vovna, *Ab initio* calculation of energy levels of trivalent lanthanide ions, *Phys. Chem. Chem. Phys.*, 2018, **20**(21), 14564–14577.
32 Y. Wei, C. Su and H. Zhang, *et al.*, Color-tunable up-conversion emission from Yb^{3+}/Er^{3+}/Tm^{3+}/Ho^{3+} codoped $KY(MoO_4)_2$ microcrystals based on energy transfer, *Ceram. Int.*, 2016, **42**(4), 4642–4647.
33 X. Zhou, G. Ju and T. Dai, *et al.*, Investigation of new color-tunable up-conversion phosphors and their long-persistent luminescence properties for potential biomedical applications, *Appl. Phys. A: Mater. Sci. Process.*, 2019, **125**, 1–8.
34 K. Lemański, R. Pązik and P. J. Dereń, Efficient up-conversion emission and energy transfer in $LaAlO_3$ doped with Er^{3+}, Ho^{3+}, and Yb^{3+} ions, *Opt. Mater.*, 2012, **34**(12), 1990–1993.
35 S. Lu, S. Yao and Q. Chen, *et al.*, Intense red upconversion emission and energy transfer in Yb^{3+}/Ho^{3+}/Er^{3+}:$CaYAlO_4$, *J. Lumin.*, 2018, **196**, 36–39.
36 S. Balaji, D. Ghosh and K. Biswas, *et al.*, Insights into $Er^{3+} \leftrightarrow Yb^{3+}$ energy transfer dynamics upon infrared ~1550 nm excitation in a low phonon fluoro-tellurite glass system, *J. Lumin.*, 2017, **187**, 441–448.
37 S. H. Jeong, Y. K. Kshetri and S. H. Kim, *et al.*, Microstructure investigation and multicolor upconversion in Yb^{3+}/Ln^{3+}(Ln = Er/Tm/Ho) ions doped α-Sialon, *Prog. Nat. Sci.: Mater. Int.*, 2019, **29**(5), 549–555.
38 A. A. Lyapin, S. V. Gushchin and S. V. Kuznetsov, *et al.*, Infrared-to-visible upconversion luminescence in SrF_2:Er powders upon excitation of the $^4I_{13/2}$ level, *Opt. Mater. Express*, 2018, **8**(7), 1863–1869.
39 X. Yin, H. Wang and T. Jiang, *et al.*, Up-conversion luminescence properties and thermal effects of $LaVO_4$:Er^{3+} under 1550 nm excitation, *Mater. Res. Bull.*, 2017, **86**, 228–233.
40 R. Lei, H. Wang and S. Xu, *et al.*, Combustion synthesis and enhanced 1.5 μm emission in Y_2O_3:Er^{3+} powders codoped with La^{3+} ions, *J. Rare Earths*, 2016, **34**(2), 125–129.
41 W. Yu, Y. Tian and M. Xing, *et al.*, Up-conversion luminescence of $NaY(WO_4)_2$:Yb, Er under 1550 and 980 nm excitation, *Mater. Res. Bull.*, 2016, **80**, 223–229.
42 A. A. Lyapin, P. A. Ryabochkina and S. V. Gushchin, *et al.*, Upconversion Luminescence of Fluoride Phosphors SrF_2:Er, Yb under Laser Excitation at 1.5 μm, *Opt. Spectrosc.*, 2018, **125**, 537–542.
43 H. Wang, M. Xing and X. Luo, *et al.*, Upconversion emission colour modulation of Y_2O_2S:Yb, Er under 1.55 μm and 980 nm excitation, *J. Alloys Compd.*, 2014, **587**, 344–348.
44 Chiho Lee, *et al.*, Origin of strong red emission in Er^{3+}-based upconversion materials: role of intermediate states and cross relaxation, *Phys. Chem. Chem. Phys.*, 2019, **21**(43), 24026–24033.
45 Hong Wang, *et al.*, Designing Er^{3+} Single-doped ternary sulfide for highly efficient upconversion luminescence under 1550 nm excitation, *Chem. Eng. J.*, 2023, **468**, 143558.
46 H. Wang, *et al.*, Upconversion emission colour modulation of Y_2O_2S:Yb, Er under 1.55 μm and 980 nm excitation, *J. Alloys Compd.*, 2014, **587**, 344–348.
47 A. Tymiński, R. M. Inocencio and G. Tomasz, Upconversion in Detail: Multicolor Emission of Yb/Er/Tm-Doped Nanoparticles under 800, 975, 1208, and 1532 nm Excitation Wavelengths, *Part. Part. Syst. Charact.*, 2020, **37**(8), 2000068.
48 X. Yin, *et al.*, Towards highly efficient NIR II response up-conversion phosphor enabled by long lifetimes of Er^{3+}, *Nat. Commun.*, 2022, **13**(1), 6549.
49 Wen Xu, *et al.*, Atomic-scale imaging of ytterbium ions in lead halide perovskites, *Sci. Adv.*, 2023, **9**(35), eadi7931.
50 Z. Li, G. Zhu and S. Li, *et al.*, High-Performance NIR Emission in Chromium-Doped Garnet Phosphors Enabled by Structure and Excitation Regulation, *Laser Photonics Rev.*, 2024, **18**(1), 2300732.
51 Z. Li, G. Zhu and S. Li, *et al.*, Ultra-small Stokes shift induced thermal robust efficient blue-emitting alkaline phosphate phosphors for LWUV WLEDs, *Ceram. Int.*, 2023, **49**(13), 21510–21520.
52 L. Yan, M. Xing and Y. Ma, *et al.*, Promising lanthanide-doped double molybdates $KYb(MoO_4)_2$ phosphors for highly efficient upconversion luminescence and temperature sensing, *Spectrochim. Acta, Part A*, 2024, **308**, 123751.
53 Y. Xu, M. Zou and H. Wang, *et al.*, Upconversion nanoparticles@ single-walled carbon nanotubes composites as efficient self-monitored photo-thermal agents, *Spectrochim. Acta, Part A*, 2023, **303**, 123173.

